

DEVELOPMENT OF A HYBRID DIRECT-INDIRECT ADAPTIVE CONTROL SYSTEM FOR THE X-33

David B. Doman *

Air Force Research Laboratory, WPAFB, OH

David B. Leggett ‡

Air Force Research Laboratory, WPAFB, OH

Anh Tuan Ngo †

Air Force Research Laboratory, WPAFB, OH

Meredith A. Saliers §

Purdue University, West Lafayette, IN

Meir Pachter ¶

Air Force Institute of Technology, WPAFB, OH

Abstract

¹ A quaternion-based attitude control system is developed for the X-33 in the ascent flight phase. A non-linear control law commands body-axis rotation rates that align the angular velocity vector with an Euler-axis defining the axis of rotation that takes the body-axis system into a desired-axis system. The magnitude of the commanded body rates are determined by the magnitude of the rotation error. The commanded body rates form the input to a dynamic inversion-based adaptive/reconfigurable control law. The indirect adaptive control portion uses on-line system identification to estimate the current control effectiveness matrix to update a control allocation module. The control allocation runs in a null-space injection mode that excites and decorrelates the effectors without degrading the vehicle response in order to enable on-line system identification. A direct adaptive control scheme uses the output of a neural network to compensate for dynamic inversion error. The overall system is designed to provide fault and damage tolerance for the X-33 on ascent. Preliminary results are shown to demonstrate the feasibility of the approach.

Introduction

Adaptive/reconfigurable flight control technologies have been maturing over the past decade. A number of different approaches have been developed

and some have been tested on fighter-type aircraft. An indirect adaptive control approach¹ was demonstrated on the VISTA-F-16 in 1995 where a simulated failure of a left horizontal tail was induced on approach and the vehicle landed without incident. More recently, the X-36 tailless remotely piloted vehicle successfully demonstrated a direct adaptive control system where a neural network was used to adaptively regulate the inversion error of a baseline dynamic inversion control law.² The Air Force RESTORE program developed a number of direct and indirect adaptive control algorithms for tailless fighter aircraft.³⁻⁶ In general, indirect adaptive control systems require on-line identification of the model parameters that are used for the on-line computation of a control law. Direct adaptive control schemes do not require explicit identification of model parameters, instead they are used to augment a certainty-equivalent control system.

Transitioning adaptive control technology to Reusable Launch Vehicles (RLVs) like the X-33 has the potential of providing benefits demonstrated on fighter aircraft to this new class of vehicle. Benefits include improved reliability through fault and damage tolerance to effector failures, and faster turnaround times through reduced flight control redesign times. The current X-33 control system is essentially a gain-scheduled PID architecture.⁷ The system is reconfigurable in that it is designed to accommodate a predefined set of failures such as engine-out, again using gain-scheduling. Adaptive-reconfigurable control is different in that the system adapts to failures (possibly unforeseen) on-line in real time. Direct adaptive flight control methods that are used to augment a dynamic inversion baseline control system are very promising and are being transitioned to the Boeing UCAV. This pa-

* Aerospace Engineer, Member AIAA

† Aerospace Engineer, Member AIAA

‡ Aerospace Engineer, Member AIAA

§ Student, Department of Aeronautics and Astronautics

¶ Professor, Department of Electrical and Computer Engineering, Senior Member AIAA

¹ This paper is declared a work of the U.S. Government and is not subject to copyright protection in the United States.

per will discuss a hybrid direct/indirect adaptive control system that is built around a baseline dynamic inversion control law. The primary function of the direct adaptive portion of the controller will be to compensate for errors or uncertainties in the base engine-aerodynamics or the non-control effector portion of the vehicle model. Dynamic inversion control laws require the use of a control effector allocation algorithm when the number of control effectors exceeds the number of controlled variables. The control allocation relies on accurate knowledge of the control derivatives. Under failure or damage conditions the control derivatives can be altered dramatically. By identifying control derivatives and supplying updated information to the control allocation block, the performance of the entire system can be improved. Thus the entire control scheme proposed here has elements of direct and indirect adaptive control. The control system described in this paper is implemented in C and interfaced with the Marshall Aerospace Vehicle Representation in C (MAVERIC)⁸ simulation of the X-33

Baseline Attitude Control System

During the ascent flight phase, the X-33 control system must track attitude commands generated by the guidance system. The use of a dynamic inversion control law to control the Euler angles of this vehicle on ascent is precluded because of the requirement to compute the Euler angle rates. The pitch attitude of the vehicle changes by more than 90 degrees throughout this flight phase which brings the well-known singularity problems inherent in the computation of Euler angle rates into play. To circumvent this problem, a quaternion-based control law is developed and coupled with a dynamic inversion-based body-axis rate command system. The system works by determining the axis of rotation that will take the vehicle's body-axis system into a desired axis system. A set of body-axis rate commands are then generated that are aligned with a body-to-desired Euler or eigen-axis. The magnitude of the commanded rates are a function of the magnitude of the scalar angular misalignment ϕ between the body and desired axis systems.

In general we define a quaternion as having scalar and vector parts:

$$\tilde{\mathbf{q}} = q_0 + \mathbf{q} = q_0 + [q_1 \quad q_2 \quad q_3] \quad (1)$$

with a constraint on the unit norm:

$$q_0^2 + q_1^2 + q_2^2 + q_3^2 = 1 \quad (2)$$

A body-to-desired quaternion $\tilde{\mathbf{q}}_{\mathbf{b}2\mathbf{d}}$ holds information about the direction of the Euler axis in its vector part $\mathbf{q}_{\mathbf{b}2\mathbf{d}}$ and information about the angular misalignment of the two axis systems in its scalar part $q_{0_{\mathbf{b}2\mathbf{d}}}$. The scalar and vector parts of the body-to-desired quaternion are given by:

$$\begin{aligned} q_{0_{\mathbf{b}2\mathbf{d}}} &= \cos(\phi/2) \\ \mathbf{q}_{\mathbf{b}2\mathbf{d}} &= \begin{bmatrix} C_1 \sin(\phi/2) \\ C_2 \sin(\phi/2) \\ C_3 \sin(\phi/2) \end{bmatrix} \end{aligned} \quad (3)$$

where C_1, C_2, C_3 are the direction cosines of the Euler axis relative to the body-axis reference frame.

The guidance system generates attitude commands referenced with respect to a plumbline-axis system. Two quaternions are used to compute the body-to-desired quaternion, the plumbline-to-desired quaternion $\tilde{\mathbf{q}}_{\mathbf{p}2\mathbf{d}}$ and the plumbline-to-body quaternion $\tilde{\mathbf{q}}_{\mathbf{p}2\mathbf{b}}$. The body-to-desired quaternion as defined above can be calculated using quaternion multiplication and inversion rules.⁹

$$\mathbf{q}_{\mathbf{b}2\mathbf{d}} = \tilde{\mathbf{q}}_{\mathbf{p}2\mathbf{b}}^{-1} \tilde{\mathbf{q}}_{\mathbf{p}2\mathbf{d}} \quad (4)$$

The vector part of $\mathbf{q}_{\mathbf{b}2\mathbf{d}}$ yields the direction of the Euler-axis in body-axis coordinates. Quaternion multiplication and inversion is a more computationally tractable approach that can be used to determine the Euler-axis and magnitude of the alignment error when compared to direction cosine matrices since the on-line computation of eigenvalues and eigenvectors and the associated sign ambiguities are side-stepped.

Figure 1 shows a conceptual block diagram of a baseline ascent attitude control system currently under development. The design is motivated by the fact that if at any instant, the body-axis angular velocity vector is aligned with the body-to-desired Euler-axis, the body-axis system will move toward the desired-axis system thereby reducing the magnitude of the attitude error. When the attitude error ϕ is zero, $q_{0_{\mathbf{b}2\mathbf{d}}} = 1$ and $\mathbf{q}_{\mathbf{b}2\mathbf{d}} = [0 \quad 0 \quad 0]$ as can be deduced from Equation 3.

Dynamic Inversion

The quaternion-based outer-loop control system generates body-axis angular velocity commands p_c, q_c, r_c that are aligned with the error Euler-axis. The inner-loop dynamic inversion control law is designed so that the X-33 tracks these body rate commands. The X-33 rotational dynamics can be written as:

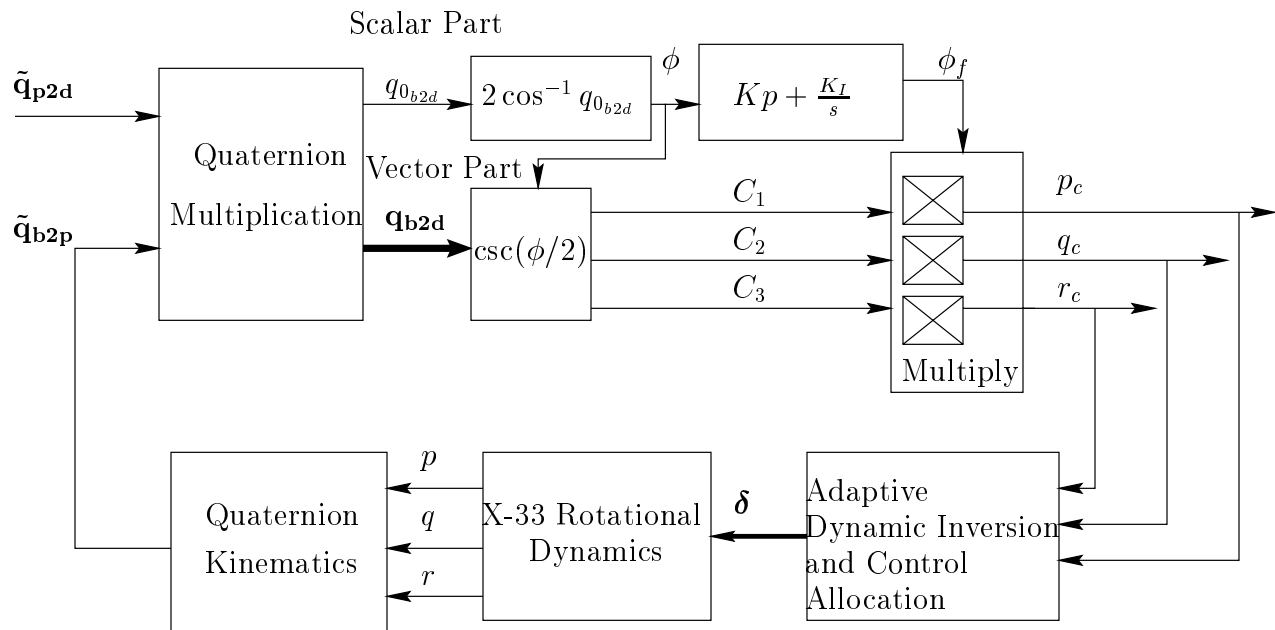


Figure 1: Conceptual Block Diagram of Quaternion-based Attitude Control System for Ascent

$$\dot{\boldsymbol{\omega}} = \mathbf{f}(\boldsymbol{\omega}, \mathbf{P}) + \mathbf{g}(\mathbf{P}, \boldsymbol{\delta}) \quad (5)$$

where $\boldsymbol{\omega} = [p \ q \ r]$ and \mathbf{P} denotes measurable or estimable quantities that influence the body rate states. The parameter \mathbf{P} includes variables such as Mach number, angle of attack, sideslip angle and vehicle mass properties such as moments of inertia. Equation 5 expresses the body-axis rotational accelerations as a sum that includes control dependent accelerations $\mathbf{g}(\mathbf{P}, \boldsymbol{\delta})$ and accelerations that are due only to the base engine and aerodynamics. It is assumed that the mass properties of the X-33 change slowly when compared to the body-axis rates so that $\dot{\mathbf{I}} \approx \mathbf{0}$ and

$$\dot{\boldsymbol{\omega}} = \mathbf{I}^{-1}(\mathbf{G}_{\mathbf{B}} - \boldsymbol{\omega} \times \mathbf{I}\boldsymbol{\omega}) \quad (6)$$

where

$$\mathbf{G}_{\mathbf{B}} = \mathbf{G}_{\text{BAE}}(\boldsymbol{\omega}, \mathbf{P}) + \mathbf{G}_{\boldsymbol{\delta}}(\mathbf{P}, \boldsymbol{\delta}) = \begin{bmatrix} \mathbf{L} \\ \mathbf{M} \\ \mathbf{N} \end{bmatrix}_{\text{BAE}} + \begin{bmatrix} \mathbf{L} \\ \mathbf{M} \\ \mathbf{N} \end{bmatrix}_{\boldsymbol{\delta}} \quad (7)$$

where $\mathbf{G}_{\text{BAE}}(\boldsymbol{\omega}, \mathbf{P})$ is the moment generated by the base engine-aerodynamic system and $\mathbf{G}_{\boldsymbol{\delta}}$ is the sum of the moments produced by the control effectors. Thus

$$\mathbf{f}(\boldsymbol{\omega}, \mathbf{P}) = \mathbf{I}^{-1}(\mathbf{G}_{\text{BAE}}(\boldsymbol{\omega}, \mathbf{P}) - \boldsymbol{\omega} \times \mathbf{I}\boldsymbol{\omega}) \quad (8)$$

and

$$\mathbf{f}(\mathbf{P}, \boldsymbol{\delta}) = \mathbf{I}^{-1}\mathbf{G}_{\boldsymbol{\delta}}(\mathbf{P}, \boldsymbol{\delta}) \quad (9)$$

Dynamic inversion requires that the control dependent portion of the model be affine in the controls. We therefore develop a linear approximation of the control dependent part such that:

$$\mathbf{G}_{\boldsymbol{\delta}}(\mathbf{P}, \boldsymbol{\delta}) \approx \mathbf{G}_{\boldsymbol{\delta}}(\mathbf{P})\boldsymbol{\delta} \quad (10)$$

The X-33 aerodynamic database provides force and moment coefficient data that is taken at a moment reference point (MRP) which is located at the center of gravity of the empty vehicle (i.e. no fuel/oxidizer). Control derivative information was extracted from the tables in the database for Mach numbers, angles of attack and sideslip angles that were to be encountered on the ascent trajectory. Polynomial fits to the discrete control derivative data were produced to provide continuous estimates of $\mathbf{G}_{\boldsymbol{\delta}}(\mathbf{P})$. The control derivatives are continuously corrected for the moving center of gravity as the vehicle ascends using the following relation:

$$\mathbf{G}_{\boldsymbol{\delta}}(\mathbf{P}) = \mathbf{G}_{\boldsymbol{\delta}_{\text{MRP}}} + (\mathbf{r}_{\text{MRP}} - \mathbf{r}_{\text{cg}}) \times \mathbf{F}_{\boldsymbol{\delta}_{\text{MRP}}} \quad (11)$$

The X-33 power pack is a XRS 2200 linear aerospike rocket engine. This engine is divided into

four quadrants: port upper A1, port lower A2, starboard upper B1 and starboard lower B2. These quadrants can be differentially throttled to generate moments that can be used for attitude control. This differential throttling is critical at launch since the aerodynamic surfaces are ineffective at low dynamic pressure. The engine control derivatives are estimated by using a global slope approximation that simply divides the estimated torque produced by a quadrant by the actual chamber pressure in that quadrant. For example, the torque gradient of the upper port quadrant A1 would be estimated by:

$$\frac{\partial \mathbf{G}_{A1}}{\partial P_{cA1}} \approx \frac{\mathbf{G}_{A1}}{P_{cA1}} \quad (12)$$

The engine control derivatives are also corrected for the moving CG. The engine torques $\mathbf{G}_{A1}, \mathbf{G}_{A2}, \mathbf{G}_{B1}, \mathbf{G}_{B2}$ are estimated by feeding chamber pressure commands through a transfer function model of the engine with limits to estimate the actual chamber pressures. The engine forces and moments are then calculated using a table lookup model parameterized by chamber pressure, mixture ratio and pressure ratio.

The model used for the design of the dynamic inversion control law becomes:

$$\dot{\boldsymbol{\omega}} = \mathbf{f}(\boldsymbol{\omega}, \mathbf{P}) + \mathbf{G}_\delta(\mathbf{P})\boldsymbol{\delta} \quad (13)$$

and our objective is to find a control law that provides direct control over $\dot{\boldsymbol{\omega}}$ so that $\dot{\boldsymbol{\omega}} = \dot{\boldsymbol{\omega}}_{des}$, i.e.

$$\dot{\boldsymbol{\omega}}_{des} = \mathbf{f}(\boldsymbol{\omega}, \mathbf{P}) + \mathbf{G}_\delta(\mathbf{P})\boldsymbol{\delta} \quad (14)$$

therefore, the inverse control must satisfy:

$$\dot{\boldsymbol{\omega}}_{des} - \mathbf{f}(\boldsymbol{\omega}, \mathbf{P}) = \mathbf{G}_\delta(\mathbf{P})\boldsymbol{\delta} \quad (15)$$

Since there are more control effectors than controlled variables, a control allocation algorithm must be used to obtain a unique solution. Control allocation will be discussed in detail in the next section. There are twelve control effectors that may be used on ascent: inboard and outboard elevons, left and right rudders, body flaps, and chamber pressures of the four quadrants of the aerospike engine. Equation 15 states that the control effectors are to be used to correct for the difference between the desired accelerations and the accelerations due only to the base engine and aerodynamic moments.

When the loop is closed around the aircraft as shown in Figure 2 and sufficient control power exists such that Equation 15 is satisfied, the transfer

function matrix should approach a bank of decoupled integrators.

$$\begin{bmatrix} p \\ q \\ r \end{bmatrix} \approx \begin{bmatrix} \frac{1}{s} & 0 & 0 \\ 0 & \frac{1}{s} & 0 \\ 0 & 0 & \frac{1}{s} \end{bmatrix} \begin{bmatrix} \dot{p}_{des} \\ \dot{q}_{des} \\ \dot{r}_{des} \end{bmatrix} \quad (16)$$

The higher the fidelity of the model used in the dynamic inversion control law, the more the closed-loop system will behave like a decoupled bank of integrators.

A command shaping prefilter is used to convert commands from the outer-loop attitude controller p_c, q_c, r_c into acceleration commands to the dynamic inversion control law $\dot{p}_{des}, \dot{q}_{des}, \dot{r}_{des}$. The prefilter structure is designed to provide a first-order low-pass filter response for each command variable $CV(p, q, r)$ to desired command variable signal $CV^{CMD}, (p_c, q_c, r_c)$. The combination of prefilter and dynamic inversion produce an implicit model following framework. Figure 3 shows a block diagram of the prefilter that is used for each axis.

The gain K_b can be interpreted as the crossover frequency of the loop transfer function. Achieving the desired closed loop dynamics is critically dependent on the dynamic inversion/control allocation algorithm successfully producing a decoupled bank of integrators. If dynamic inversion is perfect the closed-loop transfer function for each command variable becomes:

$$\frac{CV}{CV^{CMD}} = \frac{\frac{1}{2}K_B}{s + \frac{1}{2}K_B} \quad (17)$$

The gain K_B must be selected to provide sufficiently high bandwidth tracking without overdriving the control effectors.

In summary the fundamental objective of the dynamic inversion control law is to provide good body angular rate tracking. The dynamic inversion and model-following architectures will be augmented with direct and indirect adaptive control algorithms to mitigate the impact of uncertainties and compensate for damage and failures.

Control Allocation

There are three controlled variables on the ascent trajectory and twelve control effectors; therefore, a control allocation scheme must be used to ensure that Equation 15 is satisfied. The control allocation scheme used in this case draws heavily on the

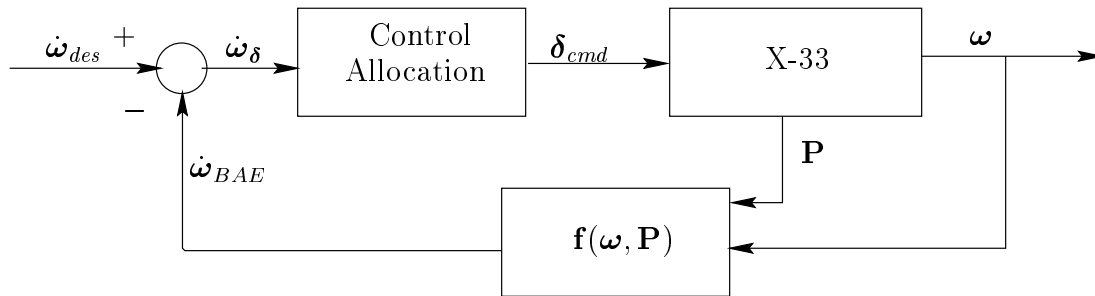


Figure 2: Block diagram of inner-loop dynamic inversion control law

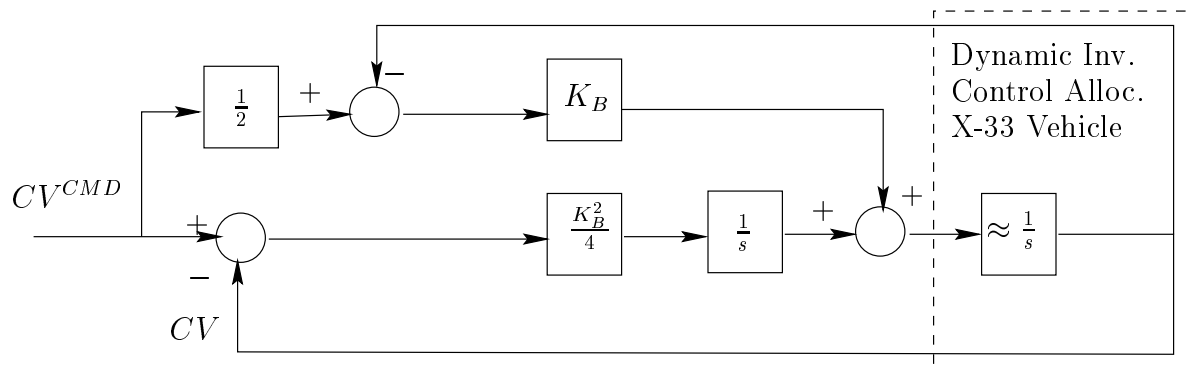


Figure 3: Implicit model following implementation using prefilter and dynamic inversion

work of Buffington et.al.^{4,10} The control allocation problems are formulated as linear programs. The LP approach minimizes a linear performance index subject to linear constraints. Numerous codes exist to solve such problems. The LP_Solve¹¹ package written in the C programming language was used in this case to be compatible with the X-33 MAVERIC simulation. Linear inequality constraints are used to ensure that effector rate and position limits are not violated. More complex engine constraints are also accommodated to ensure that feasible thrust vectoring commands are generated. The control allocation problem is broken down into a control deficiency branch and a control sufficiency branch.

Control Deficiency Branch

The control deficiency branch is used to test feasibility of satisfying Equation 15. For convenience we will refer to the left-hand side of (15) as \mathbf{d}_{des} .

$$\mathbf{d}_{des} \triangleq \dot{\omega}_{des} - \mathbf{f}(\omega, \mathbf{P}) = \mathbf{G}_{\delta}(\mathbf{P})\delta \triangleq \mathbf{B}\delta \quad (18)$$

If it is not feasible to obtain $\mathbf{d}_{des} = \mathbf{B}\delta$ due to control effector constraints, then the difference between the desired and actual effector-induced body-axis accelerations is minimized. Thus the objective can be

summarized in terms of minimizing a 1-norm performance index subject to constraints:

$$\begin{aligned} \min_{\delta} J_D &= \|\mathbf{B}\delta - \mathbf{d}_{des}\|_1 \\ \text{subject to:} & \\ \underline{\delta} &\leq \delta \leq \bar{\delta} \end{aligned} \quad (19)$$

where $\underline{\delta}$ and $\bar{\delta}$ are the most restrictive lower bounds and upper bounds on the control effector deflection.

$$\begin{aligned} \bar{\delta} &= \min(\delta_u, \Delta T \dot{\delta}_r + \delta) \\ \underline{\delta} &= \max(\delta_l, -\Delta T \dot{\delta}_r + \delta) \end{aligned} \quad (20)$$

where δ_u is the upper position limit vector, δ_l is the lower position limit vector, $\dot{\delta}_r$ is a vector of effector rate limits and ΔT is the inner-loop flight control system update rate. The optimization problem posed in Equation 19 may be transformed into the

following linear programming problem:

$$\begin{aligned} \min_{\delta} J_D = [0 \quad \cdots \quad 0 \quad 1 \quad \cdots \quad 1] \begin{bmatrix} \delta \\ \delta_s \end{bmatrix} \\ \text{subject to:} \\ \begin{bmatrix} -\delta_s \\ \delta \\ -\delta \\ \mathbf{B}\delta - \delta_s \\ -\mathbf{B}\delta - \delta_s \end{bmatrix} \leq \begin{bmatrix} \mathbf{0} \\ \bar{\delta} \\ -\underline{\delta} \\ \mathbf{d}_{\text{des}} \\ -\mathbf{d}_{\text{des}} \end{bmatrix} \end{aligned} \quad (21)$$

where δ_s which is the same dimension as the set of controlled variables. If $J_D = 0$ then the commanded controlled variable rates are achievable and there may be excess control power available that can be used to optimize sub-objectives. If $J \neq 0$, the commanded controlled variable rates are not achievable and the control allocation algorithm provides a vector of effector commands that minimize the deficiency.

Control Sufficiency Branch

If there is sufficient control power available such that $J_D = 0$, then there may be excess control power available to optimize a sub-objective. The sub-objective could involve driving the control effectors to a preferred position δ_p . A performance index reflecting this objective is given by:

$$\begin{aligned} \min_{\delta} J_S = \|\mathbf{W}_{\delta}(\delta - \delta_p)\|_1 \\ \text{subject to:} \\ \mathbf{B}\delta = \mathbf{d}_{\text{des}} \\ \underline{\delta} \leq \delta \leq \bar{\delta} \end{aligned} \quad (22)$$

where \mathbf{W}_{δ} is a vector that allows one to weight one preference over another. This optimization problem can be cast into the LP framework as follows:

$$\begin{aligned} \min_{\delta} J_S = \mathbf{W}_{\delta}^T \delta_s \\ \text{subject to:} \\ \begin{bmatrix} -\delta_s \\ \delta \\ -\delta \\ \delta - \delta_s \\ -\delta - \delta_s \end{bmatrix} \leq \begin{bmatrix} \mathbf{0} \\ \bar{\delta} \\ -\underline{\delta} \\ \delta_p \\ -\delta_p \end{bmatrix} \\ \mathbf{B}\delta = \mathbf{d}_{\text{des}} \end{aligned} \quad (23)$$

where δ , δ_s , δ_p and \mathbf{W}_{δ} are of the same dimension as the number of control effectors. The preference vector δ_p is used in this case to decorrelate the control effectors to enable on-line system identification of the control effectiveness matrix \mathbf{B} .

Null Space Injection

The indirect adaptive portion of the control law requires on-line identification of the control effectiveness matrix \mathbf{B} . This enables the control law to compensate for failures, damage or modeling errors throughout the flight. In order to identify elements of the control effectiveness matrix, each control effector must be active at all times. Furthermore, each effector must be moving independently so that there is no correlation between the movement of one control effector and another. Decorrelated control deflections are necessary to obtain a well conditioned regressor matrix for system identification. One way of doing this is to provide dithered effector commands that consist of an additive random signal that is superimposed on the nominal effector command. Unfortunately this simple approach results in degradations vehicle response since in general $\mathbf{B}(\delta + \delta_{\text{dither}}) \neq \mathbf{d}_{\text{des}}$. The solution is to provide a dithering signal that lies in the null space of the \mathbf{B} , i.e. $\mathbf{B}\delta_{\text{dither}} = \mathbf{0}$ so that $\mathbf{B}(\delta + \delta_{\text{dither}}) = \mathbf{d}_{\text{des}}$. This can be accomplished indirectly by randomly perturbing the control effector preference vector according to:

$$\delta_p \triangleq \mathbf{W}^{-1} \mathbf{B}^T (\mathbf{B} \mathbf{W}^{-1} \mathbf{B}^T)^{-1} \mathbf{d}_{\text{des}} \quad (24)$$

where

$$\begin{aligned} \mathbf{W} &= \tilde{\mathbf{W}} \mathbf{W}_r \\ \mathbf{W}_r &= \text{diag}(\mathbf{10}^{\mathbf{v}^1}, \mathbf{10}^{\mathbf{v}^2} \dots \mathbf{10}^{\mathbf{v}^m}) \end{aligned} \quad (25)$$

and \mathbf{v} is a vector of uniformly distributed random variables between -1 and 1. The matrix $\tilde{\mathbf{W}}$ is a nominal diagonal weighting matrix used for scaling purposes to equally distribute commands. Note that δ_p is actually the solution to a weighted least squares problem:

$$\begin{aligned} \min_{\delta} J = \delta^T \mathbf{W} \delta \\ \text{subject to:} \\ \mathbf{B}\delta = \mathbf{d}_{\text{des}} \end{aligned} \quad (26)$$

Thus the preference vector will be driven toward a randomly weighted least squares solution to the control allocation problem that does not account for rate and position constraints. Now the preference vector δ_p is randomly changing and the sufficiency branch of the LP-based control allocation ensures that $\mathbf{B}\delta = \mathbf{d}_{\text{des}}$ and that the control effector constraints are not violated. This approach ensures that the control effectors are decorrelated and active without degrading the vehicle response. This

approach also avoids the explicit calculation of the null space of B .

Baseline Dynamic Inversion Results

The baseline attitude control system shown in Figures 1, 2 and 3 was implemented in the MAVERIC simulation of the X-33. The roll, pitch and yaw bandwidths were set to $K_b = 5$ while the attitude error proportional and integral gains were set to $K_p = 1$ and $K_i = 0$ respectively. Null-space injection control allocation was implemented using LP techniques and was used to excite and decorrelate the control effectors without degrading the vehicle response. The commanded and actual Euler angles for the ascent trajectory are shown in Figure 4. One can see that the X-33 tracks the commanded attitude quite well. The stepped nature of the commanded attitude is a result of the slower (1 Hz) update rate of the guidance system when compared to the inner-loop flight control system (50 Hz).

The performance of the dynamic inversion control law can be more fairly evaluated by comparing the body rate commands to the actual body rates. Figure 5 makes this comparison. The actual body rates ideally should look like those of the model or low pass filtered command signals according to Equation 17. It can be seen that the actual roll and yaw rates follow the commands very closely indicating that the inversion is nearly perfect in these two axes. Small short term differences appear when comparing commanded pitch response to the actual response which indicates that some pitch-axis modeling information is inaccurate. The differences are slight however, and do not significantly impact the attitude tracking performance as can be seen in Figure 4. The appearance of high frequency noise in the pitch response is caused by the modeling error in the control effectiveness matrix and null-space injection. Integration of an on-line system identification algorithm will reduce the modeling error and allow the control allocation to adapt to control effector failures or damage.

The baseline control law operates quite well over the entire ascent trajectory which covers a very wide range of flight conditions. The vehicle is launched vertically and accelerates to approximately Mach 9.5 at 180,000 ft. The vehicle center of gravity moves approximately 4 meters as the mass of the vehicle changes from 285,000 lbm to 79,000 lbm in about 3 minutes. Note that this control law does not use gain scheduling and does not require linear models of the vehicle over the flight envelope for synthe-

sis. The control law simply requires access to the nonlinear vehicle model parameters and estimates of the vehicle states as the flight progresses. New vehicle configurations can be flown without changing the control system architecture or generating a new gain schedule. Only the new apriori estimates of the model parameters must be loaded into the flight control law.

On-Line System Identification

In the event of failures in the control surfaces, a static approach to on-line system identification proposed by Chandler et al.^{5,10} is used to estimate the vehicle's changing control derivatives. The newly updated control derivatives are then used by the dynamic inversion control law to track the attitude guidance commands. The static identification approach provides a direct, non-iterative solution. Prior information about the system such as the apriori knowledge of the effectiveness of the control surfaces can be included in the identification algorithm in the form of stochastic constraints for better estimates of these values. The control derivatives estimates can also be improved by lengthening the data window.

In this paper, a control surface failure occurs when the X-33's entire right flap δ_1 is lost at time equals 20 seconds, rendering its control derivative zero. The static identification method is used to estimate the roll control derivatives $\dot{p}_{\delta_1}, \dots, \dot{p}_{\delta_{12}}$ of the X-33's twelve control effectors $\delta_1, \dots, \delta_{12}$.

The modeled roll acceleration equation of motion in the stability axis is:

$$\begin{aligned} \dot{p} = & \dot{p}_\beta \beta + \dot{p}_r r + \dot{p}_p p + \dot{p}_{pq} pq + \dot{p}_{\delta_1} \delta_1 + \dots \\ & + \dot{p}_{\delta_{12}} \delta_{12} + w_p + \text{higher order terms} \end{aligned} \quad (27)$$

The rolling acceleration coefficients due to side-slip β , yaw rate r , roll rate p , and pitch rate p are \dot{p}_β , \dot{p}_r , \dot{p}_p , and \dot{p}_q respectively. The roll acceleration coefficients due to the twelve control effectors $\delta_1, \dots, \delta_{12}$ are $\dot{p}_{\delta_1}, \dots, \dot{p}_{\delta_{12}}$ respectively. The measurement noise is represented by w_p .

To estimate the new control derivatives, we first remove contributions of the side-slip, pitch rate, roll rate, yaw rate, and the higher order terms from (27):

$$\begin{aligned} \dot{p} = & \dot{p} - [\dot{p}_\beta \beta + \dot{p}_r r + \dot{p}_p p + \dot{p}_{pq} pq + \\ & \text{higher order terms}] = \dot{p}_{\delta_1} \delta_1 + \dots + \dot{p}_{\delta_{12}} \delta_{12} \end{aligned} \quad (28)$$

Concatenating k sampled measurements in equation (28), we have a data window of length k . Setting

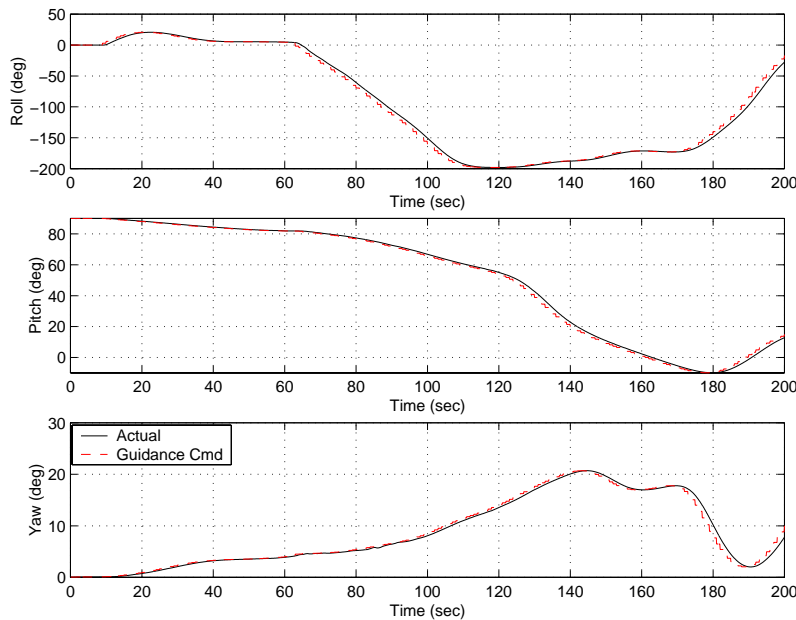


Figure 4: Attitude tracking using dynamic inversion/null-space injection control allocation

$n = 12$, the number of control effectors, we have:

$$\underbrace{\begin{bmatrix} \dot{p}_1 \\ \vdots \\ \dot{p}_k \end{bmatrix}}_Z = \underbrace{\begin{bmatrix} \delta_{1_1} & \delta_{2_1} & \cdots & \delta_{n_1} \\ \vdots & \vdots & \vdots & \vdots \\ \delta_{1_k} & \delta_{2_k} & \cdots & \delta_{n_k} \end{bmatrix}}_H \underbrace{\begin{bmatrix} \dot{p}_{\delta_1} \\ \vdots \\ \dot{p}_{\delta_n} \end{bmatrix}}_\Theta + \underbrace{\begin{bmatrix} w_{p_1} \\ \vdots \\ w_{p_k} \end{bmatrix}}_W \quad (29)$$

Compactly, equation (29) can be written as

$$Z = H\Theta + W$$

where Z denotes a $k \times 1$ vector of measured roll accelerations due to the control effectors. H is a $k \times n$ regressor matrix of measured control surface deflections. The $n \times 1$ vector Θ is the rolling moment coefficients to be estimated. The W represents the system sensor noise. The $n \times 1$ vector W is the stochastic process of zero mean with the covariance $R(\theta) = r(\theta)I_k$. The minimum-variance estimate⁵ $\hat{\Theta}_{mv}$ of Θ is then

$$\hat{\Theta}_{mv} = (H^T R^{-1} H)^{-1} H^T R^{-1} Z$$

The standard of deviation of the estimate $\hat{\Theta}$ is then:

$$\hat{\sigma} = \sqrt{(\tilde{Z}^T \tilde{Z}) / (k - n)}$$

where $\tilde{Z} = Z - H\hat{\Theta}$ is the return difference. The corresponding covariance P_{mv} of the estimate $\hat{\Theta}_{mv}$

is

$$P_{mv} = \hat{\sigma}^2 (H^T H)^{-1}$$

Apriori knowledge of parameters to be estimated, such as the values of rolling moments of the un-failed aircraft obtained from experimental tests, can be used at this point to obtain a mixed estimate of the minimum-variance estimate and apriori values. The apriori values $\Theta_{apriori}$ with its associated covariance Q becomes the stochastic constraint on the final mixed estimate $\hat{\Theta}_{me}$ and its covariance:

$$\begin{aligned} \hat{\Theta}_{me} &= \hat{\Theta}_{mv} + P_{mv} (P_{mv} + Q)^{-1} (\Theta_{apriori} - \hat{\Theta}_{mv}) \\ P_{me} &= [I - P_{mv} (P_{mv} + Q)^{-1}] P_{mv} \end{aligned}$$

In calculating the mixed estimate $\hat{\Theta}_{me}$, the $k \times n$ moving data window H is updated by replacing the earliest values of the control surface deflections with their latest values. The same is done for the $k \times 1$ vector Z of the roll accelerations. Finally, the mixed estimate results $\hat{\Theta}_{me}$ are low-pass filtered (1st order with 15 rad/sec bandwidth) to smooth out the final results.

In the example below, we apply the above identification method to estimate the control derivatives of the X-33's twelve control effectors with a complete loss of the right flap δ_1 at 20 seconds. The covariance of the effectors' apriori rolling accelerations are chosen to be $r(\delta_1) = 0.01$, and $r(\delta_1) = \cdots = r(\delta_{12}) =$

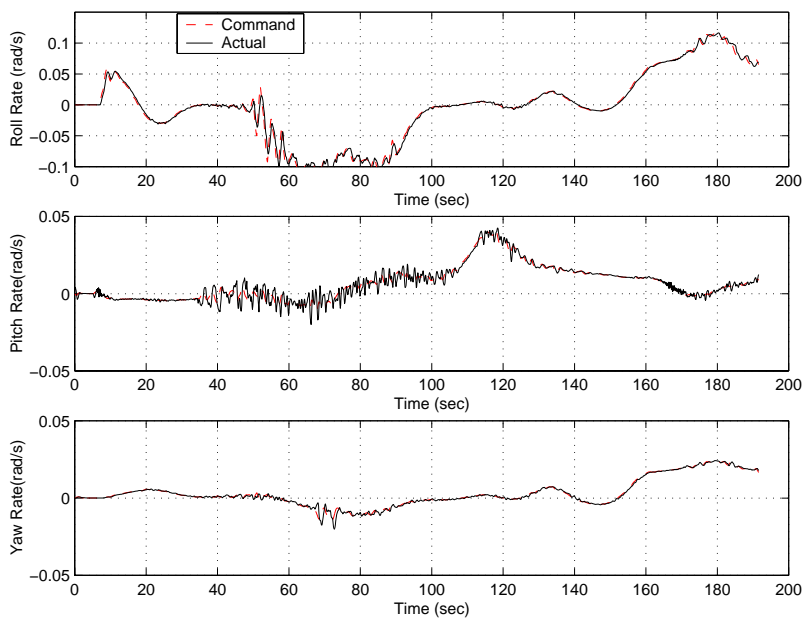


Figure 5: Body-rate tracking using dynamic inversion/null-space injection control allocation

0.0001. Figure 4 shows the nominal performance of the vehicle under no failure. With the loss of the right flap and *without* the on-line system identification the controller fails to adapt to the changing rolling moments, thus it is unable to track the guidance commands as seen in Figure 6. Under failure and *with* on-line system identification one can see that the controller is able to track the guidance commands. The value of the mixed estimate of the right flap rolling control derivative is shown in Figure 7. It is observed that rapid variation of the right flap's control derivative estimate is caused by the change in the slope of the roll command. The sensitivity of the right flap's estimate to the roll command can be reduced by choosing a slower filter. Furthermore, at lower dynamic pressure the aero control effectors $\delta_1 \cdots \delta_8$ are less effective. This occurs for time > 150 seconds. The rolling accelerations produced by the aero-effectors are thus small in equation (28) while the engine differential throttle effectors $\delta_9 \cdots \delta_{12}$ are large. This difference in the effectiveness among the vehicle's effectors cause wide fluctuations in the estimates of the aero-effectors' control derivative.

Direct Adaptive Control

Direct adaptive controllers do not require explicit identification of vehicle parameters. Instead they make use of adaptation laws that update the internal parameters in their structure and usually augment

certainly equivalent control laws such as dynamic inversion. Neural network-based adaptive control schemes have been developed by Calise¹² and Schumacher.⁶ The adaptive control architecture developed by Schumacher is used in this case since it is compatible with the baseline dynamic inversion control law described in this paper. The output of the neural network is a weighted sum of basis functions that is added to the input to the control allocation block. This adaptation signal u_{ad} is designed to cancel errors in the dynamic inversion process that arise from modeling errors. The nonlinear basis functions are formed by combining a number of different parameters p_i that are known to significantly influence the vehicle forces and moments. In this case we choose a basic family of parameters and their squares, i.e. $[1 \ p_1 \ p_1^2 \ p_2 \ p_2^2 \ \cdots]$. We then form a polynomial and cube it

$$(1 + p_1 + p_1^2 + p_2 + p_2^2 + \cdots)^3 \quad (30)$$

After expansion we remove all terms with powers greater than 2 and change all non-unity coefficients to one. Each basis function G_j is multiplied by a weight W_j that is calculated by the weight update law:

$$\dot{W}_j = -\gamma \left[\left(\frac{1}{2K_I} y + \frac{1 + K_I}{2K_p K_I} \dot{y} \right) + \eta^T [|y| \quad |\dot{y}|]^T W_j \right] \quad (31)$$

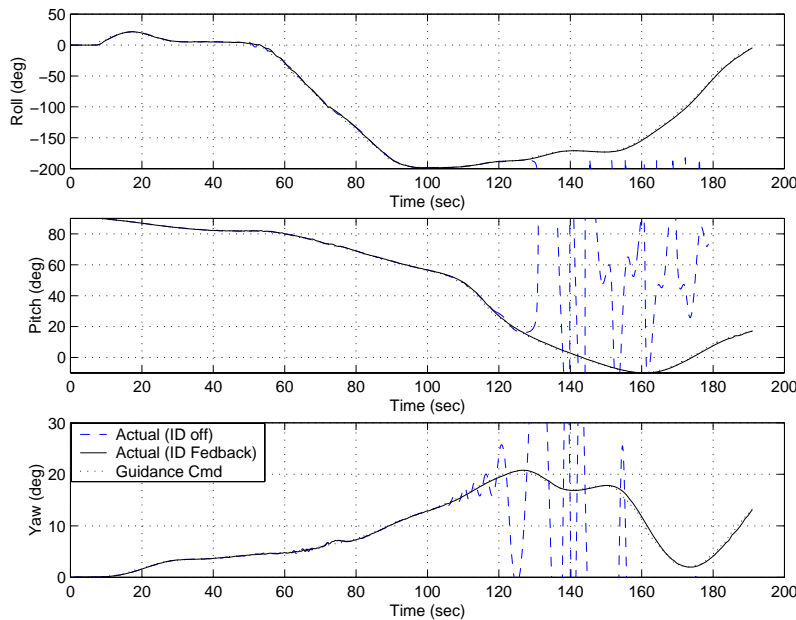


Figure 6: Attitude tracking performance with lost right flap.

where γ is the learning rate and η is similar to the “e-modification” factor that limits the growth rate of the weights. The terms K_I and K_p are related to the gain K_b in Figure 3 as follows: $K_I = \frac{K_b^2}{4}$, $K_p = K_b$. The term \dot{y} is the command variable error $CV_{model} - CV$, where CV_{model} is the output of a command filter that is an explicit model of the desired overall response. The weight update law was derived from a Lyapunov stability analysis and ensures that the time derivative of the Lyapunov function is negative definite, a necessary condition for stability. Figure 8 shows how the direct adaptive scheme fits with the baseline dynamic inversion control law. The adaptation signal for each controlled variable is obtained as follows:

$$u_{ad} = \mathbf{W}^T \mathbf{G} \quad (32)$$

where \mathbf{W} is a vector of the weights and \mathbf{G} is the vector of basis functions for the axis of interest. At the present time the basic families of parameters comprising the basis functions for each controlled vari-

able are given by:

$$\begin{aligned} \text{Roll/Yaw} \cdots & \begin{bmatrix} 1 & \alpha & \alpha^2 & \beta & \beta^2 \\ M & M^2 & p & p^2 & r \\ r^2 & \bar{q} & \bar{q}^2 & \sigma(p_\delta) & \sigma(p_\delta)^2 \\ \sigma(r_\delta) & \sigma(r_\delta)^2 & & & \end{bmatrix} \\ \text{Pitch} \cdots & \begin{bmatrix} 1 & \alpha & \alpha^2 & \beta & \beta^2 \\ M & M^2 & q & q^2 & \bar{q} \\ \bar{q}^2 & \sigma(q_\delta) & \sigma(q_\delta)^2 & & \end{bmatrix} \end{aligned} \quad (33)$$

where \bar{q} is normalized dynamic pressure and the squashing functions are defined as

$$\sigma(u) \triangleq \frac{2}{1 + e^{-0.1u}} - 1 \quad (34)$$

and has an output between -1 and 1. The remaining parameters are normalized by the magnitude of their expected maximum values.

The neural network adaptive control laws were integrated into the MAVERIC simulation and tested with learning rates of $\gamma = 20$ and $\eta = [0.01 \ 0.01]$. Test cases were produced by breaking the additive inverse $f(\boldsymbol{\omega}, P)$ loop so that no knowledge of the base engine-aerodynamics was provided to the controller. Only desired dynamics, neural network and the control allocation module were left intact. In such a situation, one would expect the output of the neural network to attempt to reconstruct the missing acceleration due to the base engine-aerodynamics.

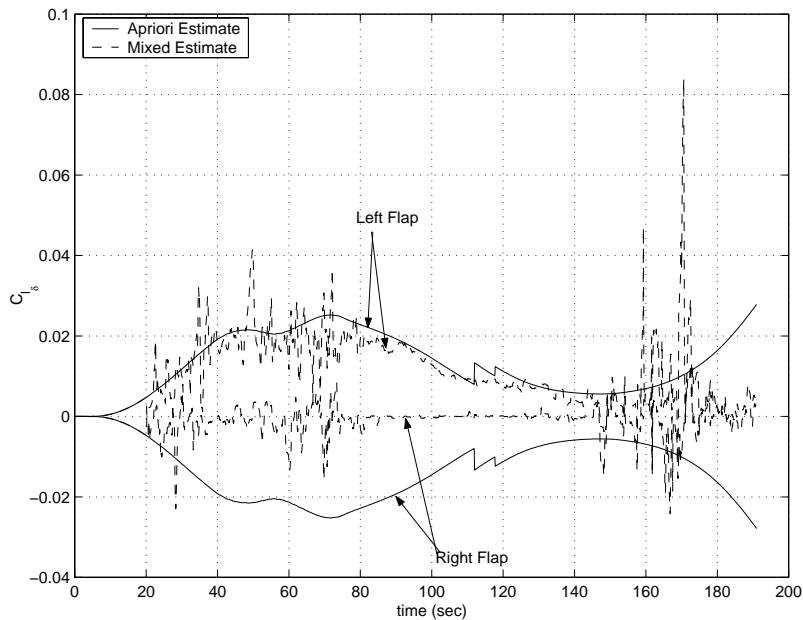


Figure 7: Apriori and mixed estimates of left and right flap roll control derivative (lost right flap, ID turned on at 20 sec)

Figure 9 compares the output of the neural network to the truth model of the base-engine aerodynamics. One can see that the two curves are quite similar which indicates that the neural network is compensating for the broken feedback loop in the roll-axis. Unfortunately, shortly before main engine cutoff (160 sec), the output of the neural network diverges and stability is lost. Similar behavior was observed for the yaw-axis network. This is particularly troublesome since the baseline dynamic inversion control law is capable of retaining good performance even with the additive inverse loops broken. The present conjecture is that the learning rate must also be made adaptive since the oscillatory divergence indicates that the learning rate is too high in some portions of the flight envelope. Richer sets of basis functions may also solve the problem and both approaches are currently under consideration.

Hybrid Adaptive Control Architecture

A block diagram of the hybrid direct/indirect adaptive control architecture for each controlled variable is shown in Figure 10. Direct and indirect adaptive components are simply modules that augment the baseline dynamic inversion/control allocation control law.

The on-line system identification module provides mixed estimates of the i 'th row of the the control

effectiveness matrix \mathbf{B}_i from measured or estimated command variable rates due to the control effectors $\dot{C}\dot{V}_{\delta_m}$ and the control effector commands. The current estimate of the \mathbf{B} matrix is used to update the control allocation. Recall that the control allocation is running in null-space injection mode to decorrelate and excite the effectors to enable on-line system ID without degrading the command variable response.

Each controlled variable uses a linear-in-parameters neural network that is primarily used to compensate for modeling error in the non-control effector portion of the X-33 moment equations. The neural networks can compensate for some control effector modeling errors as well.

On-line system ID forms the indirect adaptive component of the architecture, while the neural networks form the direct adaptive portion of the control law. The components of the control law have been through limited individual testing in the MAVERIC simulation. NASA Marshall Space Flight Center will be evaluating the control law later this fall.

Conclusions

A control architecture for the X-33 has been presented to demonstrate the feasibility of applying adaptive/reconfigurable control technologies developed for fighter aircraft to reusable launch vehicles. A baseline dynamic inversion control law with null-

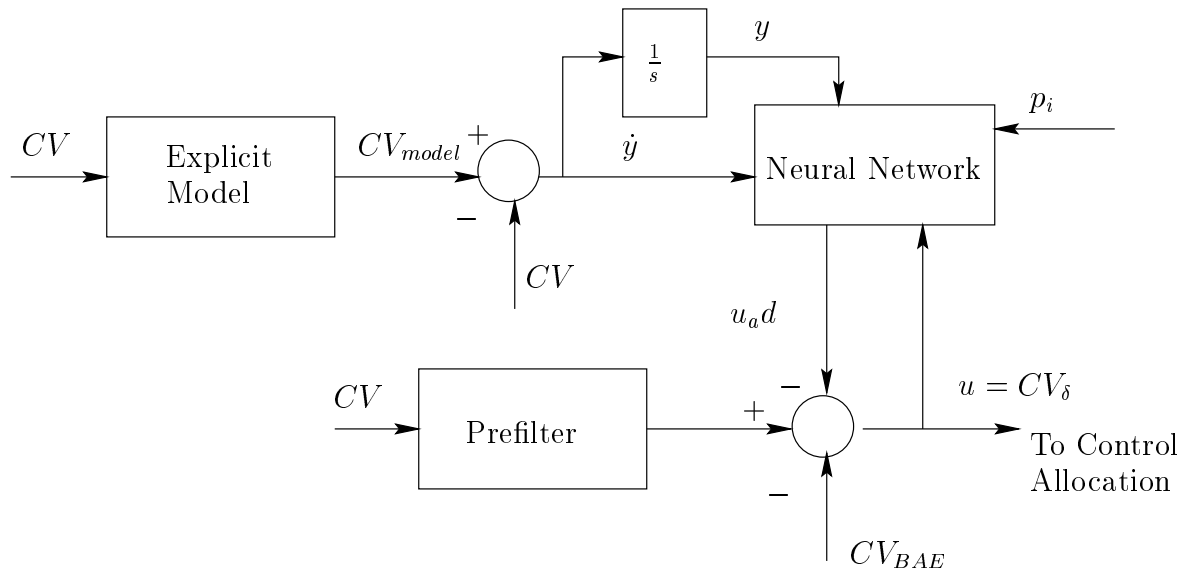


Figure 8: Integration of Neural Controller into the Dynamic Inversion Baseline

space injection control allocation demonstrated good attitude tracking capability over the entire ascent trajectory. This baseline control architecture is well suited for the insertion of direct and indirect adaptive control elements to improve the fault tolerance of these high speed flight vehicles. Dynamic inversion allows designers to easily modify the control law when vehicle configurations change or when more accurate aerodynamic data becomes available. The designer simply updates the model parameters (tables, curve-fits, etc.) and the control law synthesis is complete. Stability and robustness analyses should still be performed; however, a completed redesign of a traditional gain-scheduled control law is not necessary. The on-line system identification module has been integrated into the simulation and has been tested on a limited basis. The direct adaptive neural networks are integrated into the baseline system; however, good performance was only achieved for a limited portion of the ascent trajectory and stability was ultimately lost near main engine cutoff. The causes of the instability are under investigation. Nevertheless, the indirect adaptive portion of the control law has performed well in the limited tests that have been performed and greatly enhances the fault tolerance of the overall control law.

References

- [1] D. Ward and R. Barron, "A self-designing receding horizon optimal flight controller," in *Proceedings of the 1995 American Control Conference*, June 1995.
- [2] J. S. Brinker and K. A. Wise, "Nonlinear Simulation Analysis of a Tailless Advanced Fighter Aircraft with Reconfigurable Flight Control Law," in *Proceedings of the 1999 Guidance, Navigation and Control Conference*, AIAA 99-4040, Aug 1999.
- [3] R. L. Eberhardt, "Indirect Adaptive Flight Control of a Tailless Fighter Aircraft," in *Proceedings of the 1999 AIAA Guidance, Navigation and Control Conference*, AIAA 99-4042, Aug 1999.
- [4] J. M. Buffington, "Modular Control Law Design for the Innovative Control Effectors (ICE) Tailless Fighter Aircraft Configuration 101-3," Tech. Rep. AFRL-VA-WP-TR-1999, Air Force Research Laboratory, 1999.
- [5] M. P. Phillip R. Chandler and M. Mears, "System identification for adaptive and reconfigurable control," *Journal of Guidance, Control and Dynamics*, vol. 18, pp. 516-524, May-June 1995.
- [6] C. Schumacher, "Adaptive Flight Control Using Dynamic Inversion and Neural Networks," in *Proceedings of the 1999 AIAA Guidance, Navigation and Control Conference*, AIAA 99-4086, Aug 1999.

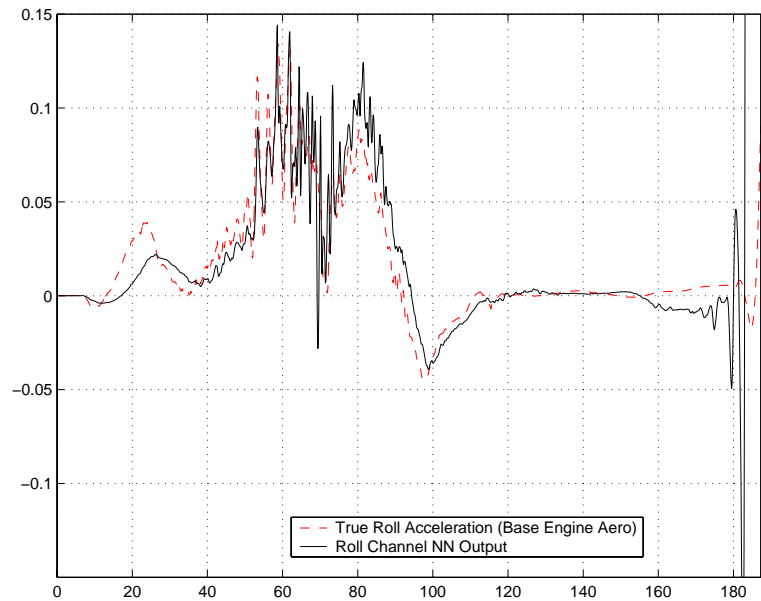


Figure 9: Roll acceleration due to base-engine-aerodynamics compared to NN output.

- [7] C. E. Hall, M. W. Gallaher, and N. Hendrix, "X-33 Attitude Control System Design for Ascent, Transition and Entry Flight Regimes," in *Proceedings of the 1998 AIAA Guidance, Navigation and Control Conference*, AIAA 98-4411, Aug 1998.
- [8] T. Dawson and J. McCarter, "Marshall Aerospace Vehicle Representation in C (MAVERIC) User's Guide," tech. rep., NASA, June 1999.
- [9] R. H. Battin, *An Introduction to the Mathematics and Methods of Astrodynamics*. New York, NY: American Institute of Aeronautics and Astronautics, 1987.
- [10] J. M. Buffington, P. Chandler, and M. Pachter, "Integration of On-line System Identification and Optimization-based Control Allocation," Tech. Rep. AIAA Paper 98-4487, American Institute of Aeronautics and Astronautics, 1998.
- [11] H. Schwab, "Documentation for lp_solve," tech. rep., University of Heidelberg Germany, 1996.
- [12] B. Kim and A. Calise, "Nonlinear flight control using neural networks," *Journal of Guidance, Control and Dynamics*, vol. 20, no. 1, pp. 26–33, 1997.

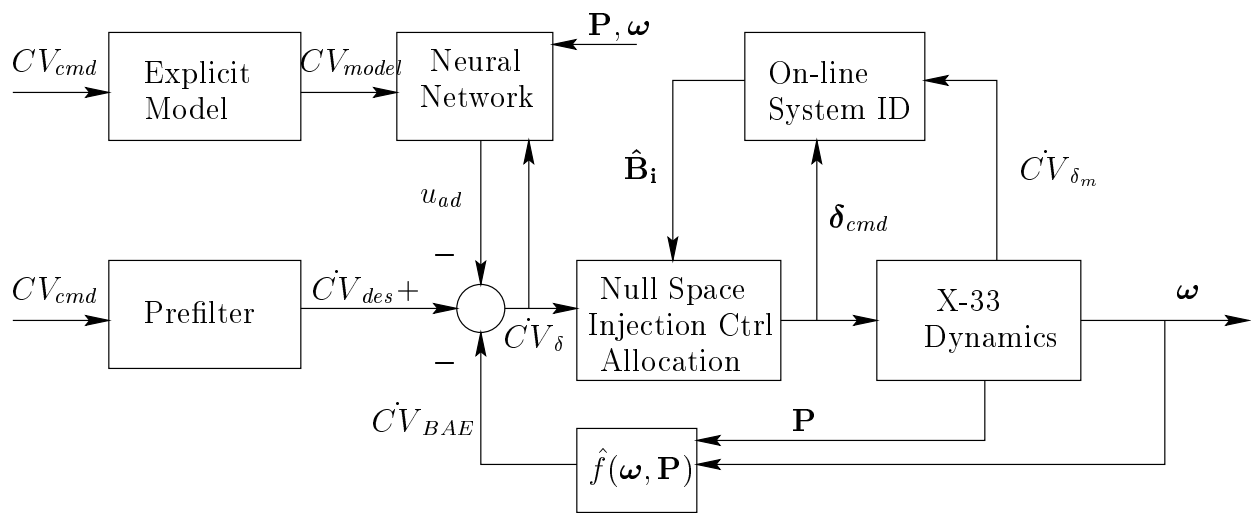


Figure 10: Block Diagram of Hybrid Direct/Indirect Adaptive Reconfigurable Control Law for X-33